PIER M

*(Received 19 March 2025, Accepted 3 July 2025, Scheduled 24 July 2025)*

# Characterization of Inhomogeneous FDM Manufactured Materials: Comparison of Free-Space and Mixing Laws

Chloé Scotti[1, *], Stefan Enoch[2], Max Groisil[1], and Nicolas Malléjac[1]

[1] *CEA, DAM, Le Ripault, F-37260 Monts, France*
[2] *Aix-Marseille Université, CNRS, Centrale Méditerranée, Institut Fresnel, Marseille 13013, France*

**ABSTRACT:** The use of additive manufacturing for the manufacturing of complex materials requires suitable characterization methods. A free-space measurement method is used for the real permittivity characterization. Depending on the considered printing pattern, the experimental result shows good agreement with theoretical values calculated using mixing laws. The setup gives promising results with characterizations of the permittivity, and it highlights the importance of taking into account the printing pattern used according to the desired effective permittivity.

## 1. INTRODUCTION

Additive manufacturing (AM) is a recent 3D printing technology that is gaining popularity in the scientific community and so has been largely developed to produce objects and materials. The speed, simplicity, and low cost of this technique has attracted a lot of interest. In particular, the manufacturing of structured and complex-shaped materials is interesting in the field of electromagnetism for the manufacturing of waveguides [1], antennas [2], or even lenses [3]. Among the different methods for AM, Fuse Deposition Modeling (FDM) [4] is one of the simplest: the material is in the form of heated wire filament deposited onto a platform, layer by layer. One of the key advantages of AM is its ability to control the structure of the material at a mesoscopic scale, which is relevant to achieving effective properties in the microwave domain.

However, this method has one disadvantage that cannot be overlooked for electromagnetic applications: the precise knowledge of the effective properties of the printed materials. Ref. [5] clearly shows that the properties of a material resulting from printing with a 100% fill parameter differ from those of the same massive material. This discrepancy is related to the microstructure of the object, which in turn depends on the manufacturing method: the presence of air inclusions in the printed material is intrinsic to the manufacturing technique and therefore influences the effective properties of the material as shown by [1]. Printing parameters such as the printing pattern have a significant impact on the effective permittivity and permeability of the material and can even participate in the creation of these unwanted inclusions [6, 7]. In addition to these difficulties, the use of additive manufacturing is becoming more complex to meet new challenges: it allows a range of effective material permittivity (or permeability) to be achieved by mixing printable materials [8] or by varying the fill rate [2, 3, 9–11]. The characterization of these materials is therefore an essential issue to be addressed. Most techniques used today to experimentally characterize the permittivity ($\varepsilon$) and permeability ($\mu$) of additively manufactured materials are destructive or require the printing of small samples. The two most widely represented types of techniques are resonant methods [5, 9, 12, 13] and waveguide methods [7, 10, 14–18]. Although these two types of characterization methods are the most accurate as demonstrated by [12], other alternative destructive methods are also developed, including microstrip characterizations [6, 19]. All these methods give a mean value of electromagnetic properties of the sample. For measuring inhomogeneous properties, the emergence of new control methods as in [20] is also worth noting. They use a resonant method for *in situ* characterization or simulation with inter-comparison with mixing laws to determine a permittivity profile in [2]. To the authors' knowledge, few studies have been dedicated to free-space Non-Destructive Techniques (NDTs) on AM materials and even fewer on materials with heterogeneous permittivity and/or permeability. This paper aims to present the result obtained using an alternative characterization method [21, 22] that brings together the last two points mentioned, namely a free-space method on intermediate-sized samples of materials with heterogeneous magneto-dielectric properties.

We will briefly present the principle of the measurement method, experimental setup, and its associated method to reconstruct the permittivity and permeability. The AM samples and their experimental characterization will then be presented, discussed, and compared to several mixing laws. This will be followed by a discussion on the relevance of the method and the importance of taking into account the microstructure to predict the effective properties of a material produced by additive manufacturing.

* Corresponding author: Chloé Scotti (chloe.scotti@etu.univ-amu.fr).

## 2. CHARACTERIZATION METHOD: MEASURING DEVICE AND ASSOCIATED METHOD

The characterization method is detailed in [21, 22]. For the purposes of this article, we will explain it without going into the details.

Characterization is based on the inversion of a diffraction problem. The considered objects are made up of strips of known geometric parameters and unknown electromagnetic parameters arranged on a metal cylinder, derived from Maxwell's equations. The model used is given by the equation presented below, which assumes the classical Born approximation of the diffraction integral equation problem.

$$\mathcal{E}_B^{\vec{mes}} - \mathcal{E}_A^{\vec{mes}} \approx -i\omega\varepsilon_0 \int (G_E) \cdot \chi_E G_E^* d\vec{r} + i\omega\mu_0 \int G_H \cdot \chi_H G_H^* d\vec{r} \quad (1)$$

The aim is to extract the contrast in dielectric $\chi_E$ and magnetic $\chi_H$ properties from which we can deduce $\varepsilon = 1+\chi_E$ and $\mu = 1+\chi_H$. For this, we obviously need to know all the other terms of the equation.

In the left member of (1), the fields $\mathcal{E}_B^{\vec{mes}}$ and $\mathcal{E}_A^{\vec{mes}}$ are obtained by measurements using the free-space characterization device in two different configurations: in configuration B when the material under test (MUT) is in the domain of interest and in configuration A when there is only the bare metal cylinder. The difference in the left member of (1) gives us the field diffracted by the MUT only.

In the right member, the only terms we need to know are the Green functions $G_E$ and $G_H$ for configuration A computed using finite element software (COMSOL MULTI-PHYSICS®).

We carry out a calibration measurement in addition to the two aforementioned measurements (configurations A and B). This allows us to calibrate the powers of the measured fields with respect to the simulated one. From the knowledge of the experimental and simulated fields, Eq.( 1) gives a linear system to be inverted to obtain $\chi_E$ and $\chi_H$.

The measuring device is a monostatic bench placed in an anechoic chamber. As shown in Fig. 1, it consists of a horn antenna operating from 2 GHz to 18 GHz and placed in front of a mobile sample holder. The antenna is connected to a Power Network Analyzer (PNA) placed outside of the chamber by coaxial cables. The antenna is placed 1 m from the center of the sample holder and positioned so that the center of its focal spot corresponds to the mid-height of the cylinder. The sample holder is a metallic cylinder with dimensions of $800 \times 124$ mm$^2$ in height and radius. The cylinder is motorized to perform a automated computer-controlled rotation $\theta$ so that MUT is illuminated from several angles, making it possible to acquire information in order to retrieve the heterogeneous properties of the MUT.

The samples are illuminated by an incident field linearly polarized parallel to the axis of revolution of the support cylinder which propagates in the $yz$ plane. In order to maximize the excitation of the sample to be measured, the MUT must be placed in an antinode of the corresponding relevant field: in a magnetic field antinode for permeability retrieval and in an electric field antinode for permittivity retrieval. A magnetic field antinode is located on the surface of the metal cylinder, and an electric field antinode is located at a distance of $\lambda/4$ from the surface of the cylinder. Some spacer devices were manufactured to place the sample at a distance $\lambda/4$ at the frequency 3.5 GHz. Therefore, characterizations are performed at this frequency. The choice of 3.5 GHz is due to a compromise between choosing a frequency far from the low operating frequency of the corner antenna used in order to obtain satisfactory antenna performance and the possibility of performing magneto-dielectric characterization; if necessary, we must place ourselves in a frequency band where possible magnetic properties could also exist [23, 24].

The setup model assumes an invariance along the $z$ axis of the metal cylinder. The properties are thus retrieved as a function of $r, \theta$. Moreover, the materials are assumed to be invariant in their thickness, so retrieval is only 1D according to the variable $\theta$ as represented on Fig. 2, with $\theta$ varying from $0°$ to $360°$. Because not the whole surface of the support is covered by materials, the measured properties are spatially inhomogeneous: the retrieved properties from $\theta = 0°$ to $\theta = 360°$ will show the values of air on each side of the value of the centered MUT (at approximately $\theta = 180°$).

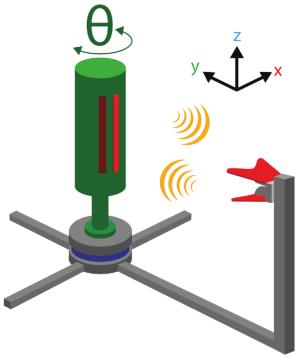


**FIGURE 1**. Sketch of the experimental setup with the transmitter-receiver antenna (gray), the sample holder (green) and multiple MUT (red) placed on the sample holder.

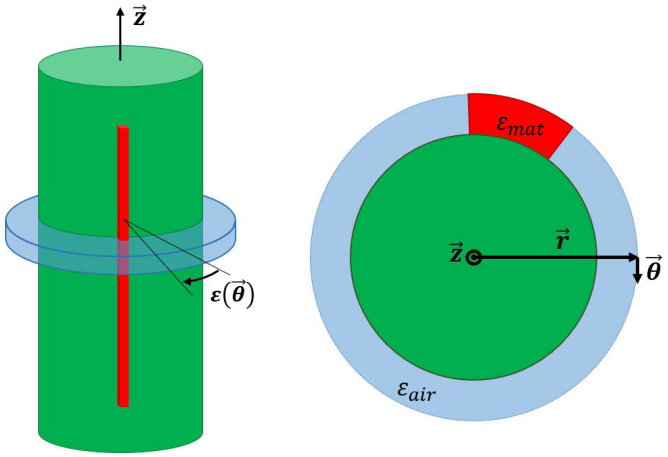


**FIGURE 2**. Sketch of the 1D model used to retrieve the permittivity. The structure is invariant along the $z$-axis and assumed homogeneous in the thickness of the sample along the $r$-axis.

In this article, the materials considered are strips made by additive manufacturing. We consider that each strip of AM material is homogeneous at the wavelength ($\lambda$) scale considered because its microstructure is sufficiently small compared to $\lambda$. By juxtaposing one or more strips around the support cylinder in this way as illustrated in Fig. 1, we obtain a artificial heterogeneous material consisting of AM strips separated by air or positioned next to each other, in other words a piecewise constant permittivity and/or permeability according to $\theta$, which we will consider as heterogeneous properties over the angular sector 0 to 360°.

The setup's ability to retrieve $\mu$ and $\varepsilon$ properties of homogeneous and heterogeneous massive materials has been determined in previous studies [21, 22]. Fig. 3 shows the characterization of two samples of bulk polylactic acid (PLA), which is a dielectric material assumed to be lossless, with different thicknesses. The real part of the materials is well reconstructed for both thicknesses. However, the imaginary part is correct only for the thinnest sample. This can be explained by the validity domain of the Born approximation. The first observed consequence of being out of this validity domain is a nonphysical increase of the imaginary part of the permittivity. This approximation is valid when measuring a weakly scattering material. The scattering power of a material increases with its geometric characteristics and its index. As can be seen in Fig. 3, at the same index but different thicknesses, too high a scattering power makes the Born approximation invalid. The validity domain of the approximation was discussed in [25]. Throughout the remainder of this article, we will use low index composites printed with lossless PLA in order to place ourselves in the conditions of validity of the Born approximation. The imaginary part will therefore no longer be exploited.

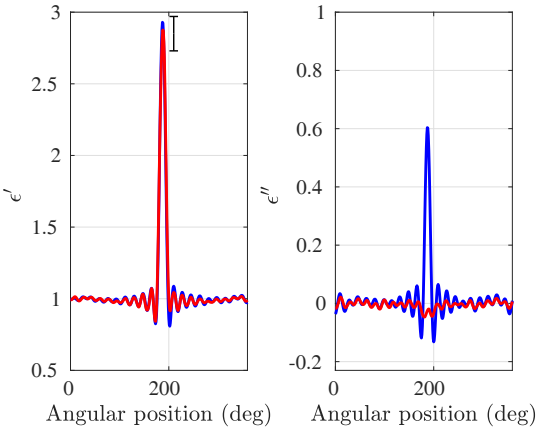


**FIGURE 3**. Reconstruction of the real part (on the left) and the imaginary part (on the right) of the permittivity of two bulk PLA test pieces produced by additive manufacturing with two different thicknesses: the 2 mm thick test piece (red) and the 5 mm thick test piece (blue). PLA considered lossless, only the real permittivity is compared to coaxial line characterization of bulk samples, represented by the error bar.

## 3. ADDITIVE MANUFACTURING AND SAMPLES

The aim of this study was to examine the material properties of objects made by additive manufacturing with an NDT method. The versatility of AM to create various material structures has been widely exploited. A panel of bulk materials combined with various meso-structures drastically enhance the possibilities for designing composite materials with a broad range of electromagnetic properties.

The manufactured samples consist of strips of printed materials. Each strip is characterized by its thickness, microstructure pattern, and material electromagnetic properties. The microstructure consists of two bulk materials: air and printed material. The effective properties of each strip can be considered as spatially constant, meaning that the microstructure is homogenizable at the considered wavelength. By arranging one or more strips on the metal cylinder support, a piecewise homogeneous material is constituted. The overall material, designated Material Under Test (MUT), is thus inhomogeneous.

The strips are made using the PRUSA slicer for a printer equipped with a 0.4 mm diameter nozzle. The structures are generated for layer heights of 100 µm and bead widths of 450 µm. The width of the unit pattern is therefore determined by the desired filling rate and bead width. To evaluate only the structure, the pattern is printed without perimeter layers (no upper, lower, left and right layer). A lower layer may however be necessary to ensure the mechanical strength of the strip due to the lack of a frame around the structure of interest (like for the H and V samples that will be defined later in this article).

The printed material used for this article is PLA of permittivity $\varepsilon = 2.8 - j0$ (and $\mu = 1 - j0$). Several strips were manufactured with this printed material: Table 1 details the characteristics of the different types of strips available.

**TABLE 1**. Manufactured strips: The first column shows the denomination of the strips which summarize its characteristics. We used 4 different filling patterns given in column 2: gyroid (G). honeycomb (N). horizontal lines (H) and vertical lines (V). Fig. 4 shows strip of each filling pattern. Column 3 gives the thickness of each strip.

| Denom | Pattern | Thickness (mm) |
|---|---|---|
| G1p-1 | gyroid | 4.6 |
| G1p-2 | gyroid | 4.6 |
| G5 | gyroid | 5 |
| G2p | gyroid | 9.2 |
| N1p | honeycomb | 4.6 |
| N2p | honeycomb | 9.2 |
| H1p | horiz | 4.6 |
| H5 | horiz | 5 |
| H2p | horiz | 9.2 |
| V1p | vert | 4.6 |
| V5 | vert | 5 |
| V2p | vert | 9.2 |

To guarantee the isotropic behavior of the gyroid, it is necessary to have a complete number of periods. Using a 0.4 mm nozzle and a 25% fill rate gives a period thickness of $p = 4.6$ mm. For all the microstructures, we chose to work on strips whose thickness is equal to one period (called 1p), to two periods (called 2p) and for some an intermediate thickness 5 mm (called 5). Strips G1p-1 and G1p-2 are two different samples

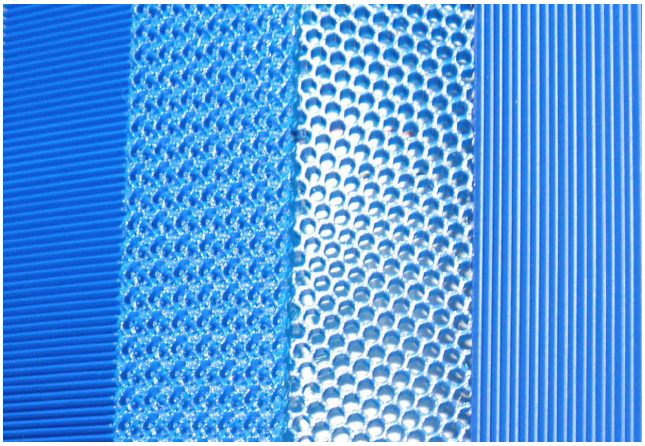

**FIGURE 4**. Photos of strips with different filling pattern, from left to right: horizontal lines (H), gyroid (G), honeycomb (N) and vertical lines (V).

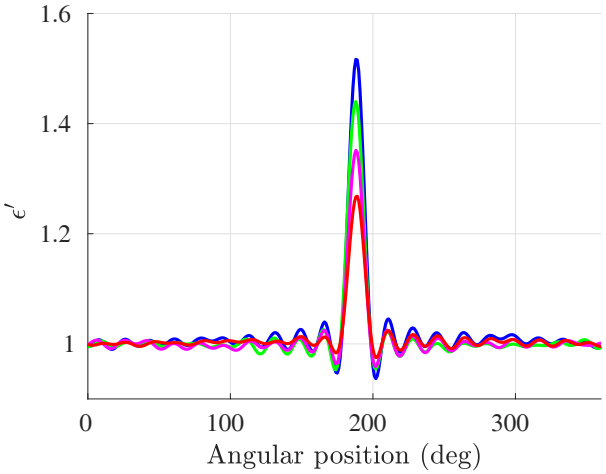


**FIGURE 5**. Reconstructed dielectric properties of 4.6 mm thick samples: V1p (dark blue), N1p (green), G1p-1 (red), G1p-2 (magenta) and H1p (red).

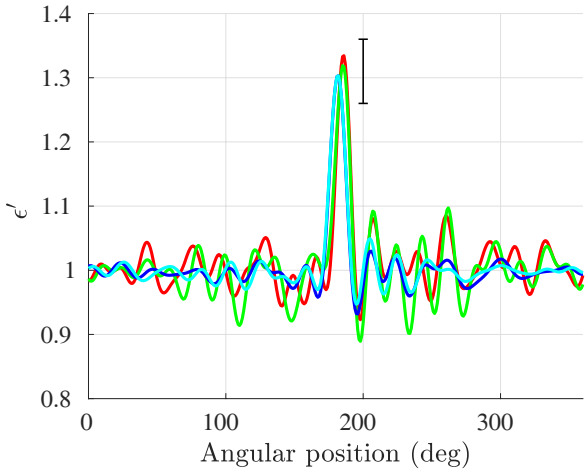


**FIGURE 6**. Reconstructed values of gyroid samples of different thickness: thickness of one period G1p-1 (red) and G1p-2 (green), thickness of two periods G2p (blue) and thickness $2 * 1$ period by the superposition G1 (p-1 + p-2) (cyan) of two samples of thickness one period. They are compared with the closest law value (M-G) and its average deviation.

(two realizations of the same theoretical material) with the same fill rate, pattern, and dimensions.

Although printing parameters and conditions can cause the appearance of air inclusions as described in [6], we assume that our structures have a sufficiently low fill rate so that the presence of possible air inclusions in the structure has a negligible impact on the quantity of printed material. We therefore assume that the volume fraction of printed material in each sample is equal to the fill rate, i.e., 25%.

## 4. RESULTS

### 4.1. Experimental Results

In this section, we present the characterizations of the strips listed in Table 1. Each characterization is the result of the 1D reconstruction of the material properties according to the angular position $\theta$ (see sketch in Fig. 2). The characterizations show one or more peaks representing the samples with air on each side. Only a few retrieval examples are shown for the discussion in the following figures.

The characterizations of the 4.6 mm thick strips are plotted in Fig. 5 for each available pattern. The characterizations of the gyroid pattern samples at all available thicknesses are shown in Fig. 6, as well as the characterization of a superposition of two 1p samples.

Finally, the characterization of a material with artificial heterogeneous permittivity is shown: this material is constructed by placing several test pieces of different patterns side by side, with a variable spacing between them.

### 4.2. Homogenization Laws

The results show that the properties are correlated to the mesoscopic structure of the material. To take into account this impact of the microstructure, we compared the results with the properties predicted by eight homogenization laws: the Wiener (W) [26] and inverse Wiener (WI) [26], Maxwell-Garnett (M-G) [27], Bruggeman (BS) [26], asymmetric Bruggeman (ABG) [28], Hashi-Shtrikman lower (HSL) and upper (HSU) limits [29], Sihvola (S) [30] and Odelevskiy (O) [31, 32] laws whose expressions are given bellow.

$$\varepsilon_W = g\varepsilon_a + (1-g)\varepsilon_b \tag{2}$$

$$\varepsilon_{WI} = \frac{\varepsilon_a\varepsilon_b}{g\varepsilon_b + (1-g)\varepsilon_b} \tag{3}$$

$$\varepsilon_{M-G} = \varepsilon_b \frac{1 + 2g\frac{\varepsilon_a-\varepsilon_b}{\varepsilon_a+2\varepsilon_b}}{1 - g\frac{\varepsilon_a-\varepsilon_b}{\varepsilon_a+2\varepsilon_b}} \tag{4}$$

$$(1-g)\frac{\varepsilon_b-\varepsilon_B}{\varepsilon_b+2\varepsilon_B} = -g\frac{\varepsilon_a-\varepsilon_B}{\varepsilon_a+2\varepsilon_B} \tag{5}$$

$$\frac{\varepsilon_a-\varepsilon_{ABG}}{\varepsilon_a-\varepsilon_b} = (1-g)\left(\frac{\varepsilon_{ABG}}{\varepsilon_b}\right)^{\frac{1}{3}} \tag{6}$$

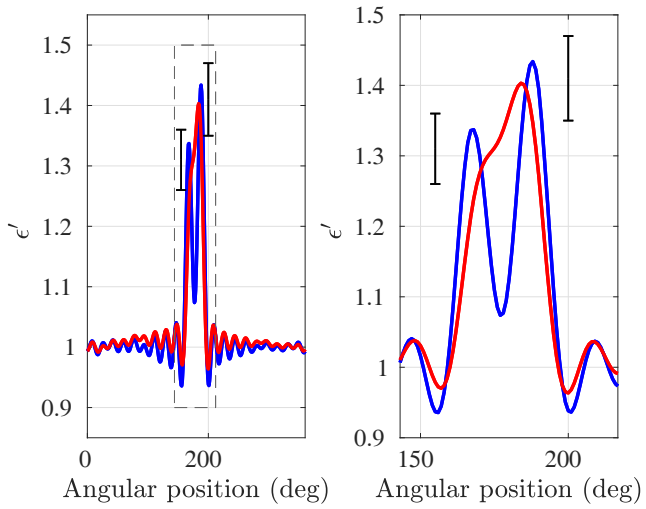


**FIGURE 7**. Reconstruction of an artificial heterogeneous material constituted of G1p and N1p. The bands are either joined (red curve) or separated by 20 mm (blue curve). A zoom is made on the central part to better observe the measured gradient of properties. The measured value of each band is compared with the closest law value and its average deviation: band G with M-G law and band N with O law

$$\varepsilon_{HS}^{L} = \varepsilon_b \frac{(1+g)\varepsilon_a + (1-g)\varepsilon_b}{(1-g)\varepsilon_a + (1+g)\varepsilon_b} \tag{7}$$

$$\varepsilon_{HS}^{U} = \varepsilon_a \frac{(2-g)\varepsilon_b + g\varepsilon_a}{g\varepsilon_b + (2-g)\varepsilon_a} \tag{8}$$

$$\frac{(1-g)(\frac{\varepsilon_S}{\varepsilon_b}-1)}{1+N(\frac{1}{p_c^S}-1)(\frac{\varepsilon_S}{\varepsilon_b}-1)} = \frac{g(\frac{\varepsilon_a}{\varepsilon_b}-\frac{\varepsilon_S}{\varepsilon_b})}{1+N(\frac{\varepsilon_a}{\varepsilon_b}-1)+N(\frac{1}{p_c^S}-1)(\frac{\varepsilon_S}{\varepsilon_b}-1)} \tag{9}$$

$$\frac{\varepsilon_O}{\varepsilon_b} - 1 = \frac{g}{N(1-\frac{g}{p_c^O}) + \frac{1}{(\frac{\varepsilon_a}{\varepsilon_b}-1)}} \tag{10}$$

with $g$ the volume fraction of 25%, $\varepsilon_a$ and $\varepsilon_b$ being respectively the permittivity of PLA and the permittivity of air, $N$ the depolarisant factor, and $p_c$ the percolation threshold filling.

Because there is a lot of homogenization laws, we chose the best-known laws that seemed most relevant to the characterized structures. W and WI correspond to linear structures and possible extremal values with respect to a linearly polarized field. MG is suitable for isotropic materials with low charge rates and spherical unit cells. B and ABG are relevant when the charge rate increases and for spherical unit cells. We looked at them because the charge rate of 25% is low but still slightly exceeds that for which MG is valid. We also chose H-S laws because many publications use the Hashin-Shtrikman model [33–37] given bellow to predict the behavior of two-phase materials such as the honeycomb pattern: walls of a first material surrounding a second material. Finally, we added the laws of S and O which follow from the modified model of that of M-G. The Sihvola law and Odelevski law are more general than other laws, but they have two supplementary parameters of the percolation threshold filling $p_c$ and depolarisant factor $N$. For certain values of the couple ($p_c$, $N$), they coincide with other laws. However, we only used some frequently used couples ($p_c$, $N$) to compare these laws with our measurement data. Because of the redundancy of results as mentioned, the only couples ($p_c$, $N$) used in the rest of this article are $(N/(1+N), \frac{1}{3})$ for S law and $(N, \frac{1}{3})$ for O law. Indeed $p_c$ and $N$ are difficult to measure for these mesostructures and even difficult to define for some of them. Using a free parameter for $p_c$, or for the couple ($p_c$, $N$), can in many case lead to a fit with an arbitrary precision but a physical meaning not easy to explain and to validate. So exploring all the potential of these general laws for the tested structure is beyond the work of this article and is still a theoretical and experimental challenge.

Table 2 shows the theoretical values calculated with each law.

**TABLE 2**. Properties of the composite material with a volume fraction of 25% according to different homogenization laws.

| Law | Calculated value |
|---|---|
| WI | 1.19 |
| HSL | 1.27 |
| M-G | 1.31 |
| ABG | 1.32 |
| BS | 1.33 |
| HSU | 1.33 |
| S | 1.34 |
| O | 1.39 |
| W | 1.45 |

## 5. DISCUSSION

### 5.1. Characterization of a Single Strip

Table 3 shows all the measured properties and the nearest value obtained with the different homogenization laws and gives the deviation with the results of each mixing law. We assume that the difference between the experimental values for each pattern originates from a variation in the position of the sample on the measuring bench or from the calibration measurement carried out at each material measurement.

Table 3. Comparison between the experimental value of single-band material and homogenization laws. The 'D25' of the denomination has been removed. The deviations found are negative or positive depending on whether the experimental value is lower or higher than the calculated value. Values in red represent the smallest deviation between the measured value and the calculated one. The law giving the nearest value is precised in the last column. Rectangles in bright colors delimit the domain including all the nearest values for each pattern.

| Sample | Meas. | WI | HSL | MG | ABG | BS | HSU | S | O | W | Nearest |
|---|---|---|---|---|---|---|---|---|---|---|---|
| G1(p-1+p-2) | 1,31 | 9,16 % | 3,05 % | 0,00 % | -0,76 % | -1,53 % | -1,53 % | -2,29 % | -6,11 % | -10,69 % | MG |
| G1p-1 | 1,30 | 8,46 % | 2,31 % | -0,77 % | -1,54 % | -2,31 % | -2,31 % | -3,08 % | -6,92 % | -11,54 % | MG |
| G1p-1 | 1,33 | 10,53 % | 4,51 % | 1,50 % | 0,75 % | 0,00 % | 0,00 % | -0,75 % | -4,51 % | -9,02 % | BS/HSU |
| G1p-2 | 1,35 | 11,85 % | 5,93 % | 2,96 % | 2,22 % | 1,48 % | 1,48 % | 0,74 % | -2,96 % | -7,41 % | S |
| G2p | 1,30 | 8,46 % | 2,31 % | -0,77 % | -1,54 % | -2,31 % | -2,31 % | -3,08 % | -6,92 % | -11,54 % | MG |
| G2p | 1,32 | 9,85 % | 3,79 % | 0,76 % | 0,00 % | -0,76 % | -0,76 % | -1,52 % | -5,30 % | -9,85 % | ABG |
| G5 | 1,31 | 9,16 % | 3,05 % | 0,00 % | -0,76 % | -1,53 % | -1,53 % | -2,29 % | -6,11 % | -10,69 % | MG |
| G5 | 1,29 | 7,75 % | 1,55 % | -1,55 % | -2,33 % | -3,10 % | -3,10 % | -3,88 % | -7,75 % | -12,40 % | MG |
| H1p | 1,27 | 6,30 % | 0,00 % | -3,15 % | -3,94 % | -4,72 % | -4,72 % | -5,51 % | -9,45 % | -14,17 % | HSL |
| H1p | 1,22 | 2,46 % | -4,10 % | -7,38 % | -8,20 % | -9,02 % | -9,02 % | -9,84 % | -13,93 % | -18,85 % | WI |
| H1p | 1,24 | 4,03 % | -2,42 % | -5,65 % | -6,45 % | -7,26 % | -7,26 % | -8,06 % | -12,10 % | -16,94 % | HSL |
| H1p | 1,26 | 5,56 % | -0,79 % | -3,97 % | -4,76 % | -5,56 % | -5,56 % | -6,35 % | -10,32 % | -15,08 % | HSL |
| H1p | 1,17 | -1,71 % | -8,55 % | -11,97 % | -12,82 % | -13,68 % | -13,68 % | -14,53 % | -18,80 % | -23,93 % | WI |
| H2p | 1,17 | -1,71 % | -8,55 % | -11,97 % | -12,82 % | -13,68 % | -13,68 % | -14,53 % | -18,80 % | -23,93 % | WI |
| H2p | 1,19 | 0,00 % | -6,72 % | -10,08 % | -10,92 % | -11,76 % | -11,76 % | -12,61 % | -16,81 % | -21,85 % | WI |
| H5 | 1,24 | 4,03 % | -2,42 % | -5,65 % | -6,45 % | -7,26 % | -7,26 % | -8,06 % | -12,10 % | -16,94 % | HSL |
| N1p | 1,40 | 15,00 % | 9,29 % | 6,43 % | 5,71 % | 5,00 % | 5,00 % | 4,29 % | 0,71 % | -3,57 % | O |
| N1p | 1,43 | 16,78 % | 11,19 % | 8,39 % | 7,69 % | 6,99 % | 6,99 % | 6,29 % | 2,80 % | -1,40 % | W |
| N2p | 1,38 | 13,77 % | 7,97 % | 5,07 % | 4,35 % | 3,62 % | 3,62 % | 2,90 % | -0,72 % | -5,07 % | O |
| V1p | 1,52 | 21,71 % | 16,45 % | 13,82 % | 13,16 % | 12,50 % | 12,50 % | 11,84 % | 8,55 % | 4,61 % | W |
| V1p | 1,55 | 23,23 % | 18,06 % | 15,48 % | 14,84 % | 14,19 % | 14,19 % | 13,55 % | 10,32 % | 6,45 % | W |
| V1p | 1,55 | 23,23 % | 18,06 % | 15,48 % | 14,84 % | 14,19 % | 14,19 % | 13,55 % | 10,32 % | 6,45 % | W |
| V2p | 1,43 | 16,78 % | 11,19 % | 8,39 % | 7,69 % | 6,99 % | 6,99 % | 6,29 % | 2,80 % | -1,40 % | W |
| V5 | 1,50 | 20,67 % | 15,33 % | 12,67 % | 12,00 % | 11,33 % | 11,33 % | 10,67 % | 7,33 % | 3,33 % | W |

Figure 5 shows that, depending on the printing pattern used, with the same volume fraction and the same printed bulk material properties, the composite material effective properties are different. The permittivity values of the MUTs are (from the lowest to the highest): first the Hlp, then the Glp, then the N1p, and finally the H1p. It is well known that patterns with horizontal (resp. vertical) lines are supposed to interact the least (resp. the most) with the incident field (which is linearly polarized): as expected they are the extrema of the measured values. The other patterns are consistently intermediate between these two extreme anisotropic cases. This hypothesis is confirmed by the homogenization laws. Indeed, as said earlier, Wiener's laws are usually used to calculate the extrema of possible values in homogenization laws. We can clearly see that the H and V samples have their reconstructed values closer to Wiener's laws with a respective average deviation of 2.63% and 4.45%. The H pattern gives experimental results close to two laws: WI and HSL. We expect to obtain results close exclusively to WI. We explain this observation by the poor mechanical strength of the sample: due to the lack of an external frame, the sample is very flexible, which can cause its position to deviate during the rotation of the support and therefore result in a poor assessment of its permittivity. The V-pattern samples are the most rigid among the available samples. The experimental values are all close to those calculated by the W law but overestimate it, which seems inconsistent since the Wiener's laws are supposed to frame the possible property values for a given volume fraction. We consider that this result comes from exceeding the limits of the Born approximation for the dimensions of the samples and the theoretical value of the material index, which we take here as the value of the Wiener's law, as described in Section 2 and in [21, 22]. However, we consider that the average deviation remains acceptable. The gyroid pattern gives measured values close to those calculated by the M-G law, which is consistent with the low charge rate and M-G hypothesis. It is also the pattern that gives the measured results with the lowest deviation: 0.57% on average. The other laws translating isotropic behavior (ABS, BS, HSU) generally have calculated values very close to the experimental ones. The values calculated with the S and O laws are, however, not very close although these laws are derived from the Maxell-Garnett model. The characterizations of the N strips seem surprising. Indeed, we expected experimental values in agreement with the HSL or HSU homogenization laws because this pattern is supposed

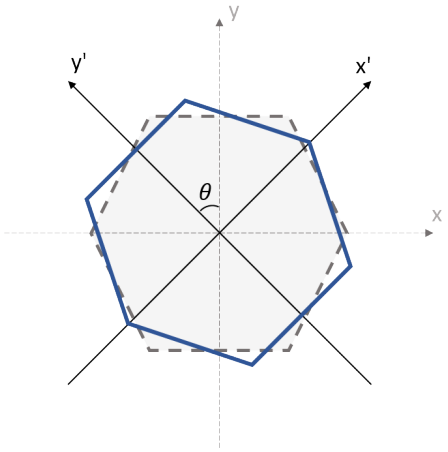


**FIGURE 8**. Sketch of the tilting of the pattern honeycomb of $\theta = 45°$ relative to the reference positioning shown in dotted lines.

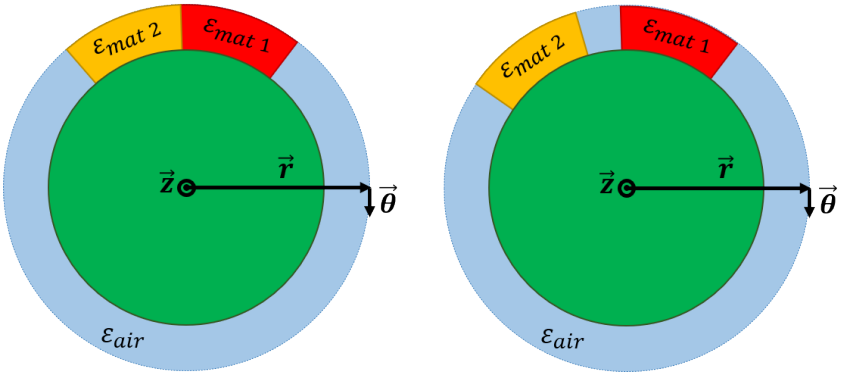


**FIGURE 9**. Illustration of the two configurations used for the two strips characterization: on the left the edge-by-edge configuration and on the right the 20 mm spaced configuration.

to account for an isotropic material, and these laws represent them best. However, all experimental values are greater than the upper limit of H-S model, and we see that the experimental results are closer to the value of the O law. Several hypotheses have been raised to explain this observation. First of all, the assumptions of H-S are that the unit cell is comparable to a sphere and so has an isotropic behavior, which is consistent with the approximations of the M-G models and its S and O derivatives. It is therefore understandable that the value calculated by the O law is close to the experimental value. Secondly, the more the material index increases, the more the measurement means tend to overestimate the permittivity of the MUT as can be seen during the characterization of the V strips. The second hypothesis, on the other hand, concerns the legitimacy of the approximations made that lead to the use of H-S [29]: indeed, this assumes that the apparent macroscopic isotropy gives $\varepsilon_x = \varepsilon_y \equiv \varepsilon_t$, which means that the permittivity is the same in every direction considered, and that the shape of the internal material, here air, can be approximated by a sphere. If these approximations are no longer valid [38, 39], then we question the relevance of using this model in our case. Indeed, for reasons of mechanical strength, the honeycomb pattern used was inclined at $45°$ relative to the reference axis $xy$ as can be seen in Fig. 8. Thus, we can question the equality statement $\varepsilon_x = \varepsilon_y = \varepsilon_{x'} = \varepsilon_{y'} \equiv \varepsilon_t$ with an illumination polarized in the $y$ direction.

Further work appears necessary to investigate these two hypotheses.

On another point, Fig. 6 also shows that by increasing the thickness of the specimens up to 9.2 mm (enabling a whole number of periods to be kept), the reconstructed values are very similar to those found for the 4.6 mm thick samples. Thus, the values obtained can be considered as intrinsic properties of the composite material. However, we notice in Table 3 that the greater the thickness of the samples is, the smaller the deviations from the theoretical laws are, whatever the pattern. We can conclude that our samples are representative of the composite materials, but that an optimization of their dimensions could improve the accuracy of the characterization.

Experimental values may be close to several calculated values, and although we can identify a law with the closest values on average, the deviation of the experimental values caused by the calibration process and the placement of the sample does not allow us to discretize the most relevant distribution according to the MUT pattern. However, we note that for each pattern, Table 3 highlights that the groups of laws giving calculated values close to the experimental values have similar or even identical assumptions and approximations. This results in close calculated values within the same group of laws. Depending on the calibration measurement performed or the positioning of the sample, the experimental value should therefore be included in this group of calculated values. However, Table 3 shows that our measurement method has an average deviation of 2.63% with the closest average law without any a priori geometric shape or properties.

### 5.2. Characterization of Heterogeneous Materials

Another heterogeneous dielectric material was artificially constructed using two strips. The constructed material therefore has piecewise varying properties. Each section characterization can be considered as a strip characterization. Thus, characterization results will be compared to the result of the most pertinent law as determined in the previous section. Fig. 7 shows two configurations using a G1p and a N1p: they are either placed edge-by-edge on their long side or spaced 20 mm apart as illustrated in Fig. 9. The gradient of properties is well detected, and the reconstructed permittivity values are included in the confidence interval which is calculated for each pattern with the closest calculated value more or less the average deviation.

It can be noted that the reconstructed permittivity between the two strips when they are separated is not that of air but close to the latter. The combination of the measuring setup and inversion method makes it possible to obtain a spatial resolution to separate two strips by approximately $\lambda/3$. This is due to classical oscillations observed in near-field/far field transformation of sharp sources. Thus, it is associated with the sharp discontinuities of material properties (between strips and air).

When the strips are placed edge-by-edge, the angular resolution is insufficient to clearly distinguish the two strips. However, the reconstruction shape shows an inflection point corresponding to the lower-level strip (on the left on the red curve).

By calculating the angular difference between this inflection point and the top of the peak on the right, we obtain $L = \frac{\Delta\theta * \pi * R}{180} = 30$ mm with $R$ being the radius of the support which corresponds to the distance between the two strip centers.

## 6. CONCLUSION

We have shown that free-space techniques have their place in the characterization of complex AM materials. It has been shown that it is important to consider the printing pattern and the illumination used by the device. Indeed, as demonstrated by [6], the variation of the effective permittivity value of the strips is not negligible depending on the printing pattern and this even for bands with controlled volume fraction (permitted by AM). Furthermore, the experimental values match the values defined by adapted mixing laws with a small average deviation. The device seems to represent an appropriate nondestructive FA characterization technique.

## REFERENCES


[1] Baer, C., "A compensation method for reducing the influence of printing voids on the wave propagation properties of FDM-manufactured dielectric waveguides," in *2024 International Conference on Electromagnetics in Advanced Applications (ICEAA)*, 89–93, Lisbon, Portugal, 2024.

[2] Hehenberger, S. P., S. Caizzone, and A. G. Yarovoy, "Additive manufacturing of linear continuous permittivity profiles and their application to cylindrical dielectric resonator antennas," *IEEE Open Journal of Antennas and Propagation*, Vol. 4, 373–382, 2023.

[3] Vial, B., H. Giddens, and Y. Hao, "Multi-material additive manufacturing of microwave devices," in *2022 16th European Conference on Antennas and Propagation (EuCAP)*, 1–5, Madrid, Spain, 2022.

[4] Kristiawan, R. B., F. Imaduddin, D. Ariawan, Ubaidillah, and Z. Arifin, "A review on the fused deposition modeling (FDM) 3D printing: Filament processing, materials, and printing parameters," *Open Engineering*, Vol. 11, No. 1, 639–649, 2021.

[5] Colella, R., F. P. Chietera, A. Michel, G. Muntoni, G. Casula, G. Montisci, and L. Catarinucci, "Electromagnetic characterisation of conductive 3D-Printable filaments for designing fully 3D-Printed antennas," *IET Microwaves, Antennas & Propagation*, Vol. 16, No. 11, 687–698, 2022.

[6] Persad, J. and S. Rocke, "Impact of 3D printing infill patterns on the effective permittivity of 3D printed substrates," *IEEE Journal of Microwaves*, Vol. 4, No. 2, 277–292, 2024.

[7] Gözüm, A., M. Bakir, and O. Akgöl, "Electromagnetic characterization of 3D printed metamaterial absorber with conductive paint," *Journal of Additive Manufacturing Technologies*, Vol. 2, No. 1, 706–706, 2022.

[8] De Oliveira Neto, A. M., J. F. Justo, W. Beccaro, and A. M. de Oliveira, "Designing and building radio frequency devices with tailored dielectric properties using additive manufacturing," *Microwave and Optical Technology Letters*, Vol. 65, No. 3, 777–784, 2023.

[9] Alimenti, A., N. Pompeo, K. Torokhtii, E. Pittella, E. Piuzzi, and E. Silva, "A system to measure the complex permittivity of 3D-printing materials," in *2022 IEEE International Conference on Flexible and Printable Sensors and Systems (FLEPS)*, 1–4, Vienna, Austria, 2022.

[10] Andersson, S., "Feasibility study on additive manufacturing of dielectrics in antenna structures," Master thesis, Aalto University, Espoo, Finland, 2023.

[11] Nguyen, T. A., "Electromagnetic properties of 3D printing materials," Master's thesis, Tampere University, Tampere, Finland, 2024.

[12] Ghodgaonkar, D. K., V. V. Varadan, and V. K. Varadan, "Free-space measurement of complex permittivity and complex permeability of magnetic materials at microwave frequencies," *IEEE Transactions on Instrumentation and Measurement*, Vol. 39, No. 2, 387–394, 1990.

[13] Migalin, M. M., A. V. Kovalev, S. R. Gadzhiev, V. S. Kuzmin, L. N. Libin, and V. A. Fleyteng, "Complex dielectric permittivity measurement of 3D printing resin FTD nano clear in the 1-10 GHz band," in *2023 Seminar on Microelectronics, Dielectrics and Plasmas (MDP)*, 82–85, Saint Petersburg, Russian Federation, 2023.

[14] Deffenbaugh, P. I., R. C. Rumpf, and K. H. Church, "Broadband microwave frequency characterization of 3-D printed materials," *IEEE Transactions on Components, Packaging and Manufacturing Technology*, Vol. 3, No. 12, 2147–2155, 2013.

[15] Fessaras, T., Z. Larimore, P. Parsons, K. Nicholson, and M. Mirotznik, "Custom hopper fed additive manufacturing system for printing high permittivity materials and radio frequency structures," *Available at SSRN 4603609*, 2024.

[16] Filbert, J., A. Barvincak, M. T. A. Qaseer, and R. Zoughi, "Microwave characterization of metal powder in additive manufacturing (AM)," *IEEE Open Journal of Instrumentation and Measurement*, Vol. 3, 1–13, 2024.

[17] Kattel, B., U. Ayan, M. Mohoppu, B. Villacorta, and W. E. Hutchcraft, "Enhancing permittivity of 3D printing filaments via nanocompounding for electromagnetic applications," in *SoutheastCon 2024*, 1016–1021, Atlanta, GA, USA, 2024.

[18] Raj, R., A. P. Moharana, and A. R. Dixit, "Design and fabrication of flexible woodpile structured nanocomposite for microwave absorption using material extrusion additive technique," *Additive Manufacturing*, Vol. 79, 103935, 2024.

[19] Pérez-Escribano, M., "Characterization techniques for microwave and millimeter-wave circuit design using additive manufacturing and multiconductor transmission lines," Ph.D. dissertation, University of Málaga, Málaga, Andalusia, Spain, 2022.

[20] Lekas, S., R. Drummond, P. S. Grant, and S. R. Duncan, "Control of additive manufacturing for radio frequency devices with spatially varying dielectric properties," *IEEE Transactions on Control Systems Technology*, Vol. 32, No. 5, 1579–1589, 2024.

[21] Faget, X., A. Litman, E. Dieudonné, S. Enoch, and N. Malléjac, "Free-space characterization of the permeability of inhomogeneous magneto-dielectric materials," *IEEE Transactions on Microwave Theory and Techniques*, Vol. 65, No. 12, 5035–5045, 2017.

[22] Scotti, C., K. Aït-Otmane, F. Duverger, M. Groisil, P. Jomin, S. Enoch, A. Litman, and N. Malléjac, "Non-destructive characterization of magneto-dielectric materials using a born approximation model," in *2023 IEEE Conference on Antenna Measurements and Applications (CAMA)*, 78–81, Genoa, Italy, 2023.

[23] Han, M. and Y. Jiang, "Gigahertz permeability of Fe-Cu-Nb-Si-B ferromagnetic microwires and micromagnetics simulations," *Materials Today Communications*, Vol. 38, 107693, 2024.

[24] Rozanov, K. N., Z. W. Li, L. F. Chen, and M. Y. Koledintseva, "Microwave permeability of Co2Z composites," *Journal of Applied Physics*, Vol. 97, No. 1, 013905, 2005.

[25] Scotti, C., M. Groisil, M. Latrach, A. Litman, S. Enoch, and N. Malléjac, "Imagerie quantitative de matériaux magnéto

diélectriques hétérogènes: Validité de l'approximation de born et pertes par diffusion," *23ème Journées Nationales Microondes 2024*, 2024.

[26] Karkkainen, K. K., A. H. Sihvola, and K. I. Nikoskinen, "Effective permittivity of mixtures: Numerical validation by the FDTD method," *IEEE Transactions on Geoscience and Remote Sensing*, Vol. 38, No. 3, 1303–1308, 2000.

[27] Choy, T. C., *Effective Medium Theory: Principles and Applications*, Oxford University Press, 2015.

[28] Merrill, W. M., R. E. Diaz, M. M. LoRe, M. C. Squires, and N. G. Alexopoulos, "Effective medium theories for artificial materials composed of multiple sizes of spherical inclusions in a host continuum," *IEEE Transactions on Antennas and Propagation*, Vol. 47, No. 1, 142–148, 1999.

[29] Hashin, Z. and S. Shtrikman, "A variational approach to the theory of the effective magnetic permeability of multiphase materials," *Journal of Applied Physics*, Vol. 33, No. 10, 3125–3131, 1962.

[30] Sihvola, A. H. and J. A. Kong, "Effective permittivity of dielectric mixtures," *IEEE Transactions on Geoscience and Remote Sensing*, Vol. 26, No. 4, 420–429, 1988.

[31] Odelevskiy, V. I., "Calculation of the generalized conductivity of heterogeneous systems," *Zh. Tekh. Fiz*, Vol. 21, No. 6, 678–685, 1951.

[32] Starostenko, S. N., K. N. Rozanov, V. Bovtun, and A. O. Shiryaev, "A mixing formula accounting for inversion of matrix structure," *AIP Advances*, Vol. 10, No. 1, 015115, 2020.

[33] Johansson, M., C. L. Holloway, and E. F. Kuester, "Effective electromagnetic properties of honeycomb composites, and hollow-pyramidal and alternating-wedge absorbers," *IEEE Transactions on Antennas and Propagation*, Vol. 53, No. 2, 728–736, 2005.

[34] Ma, L. and Q. Yang, "On the homogenization analysis of electromagnetic properties for irregular honeycombs," *CMC — Computers Materials & Continua*, Vol. 40, No. 2, 79–97, 2014.

[35] Liu, L., C. Fan, N. B. Zhu, Z. Y. Zhao, and R. P. Liu, "Effective electromagnetic properties of honeycomb substrate coated with dielectric or magnetic layer," *Applied Physics A*, Vol. 116, 901–905, 2014.

[36] Zhao, Y.-C., J.-F. Liu, Z.-G. Song, and X.-L. Xi, "Novel closed-form expressions for effective electromagnetic parameters of honeycomb radar-absorbing structure," *IEEE Transactions on Antennas and Propagation*, Vol. 64, No. 5, 1768–1778, 2016.

[37] Qiu, K., S. Feng, C. Wu, Z. Liu, *et al.*, "Calculation of effective permittivity and optimization of absorption property of honeycomb cores with absorbing coatings," *Materials Science*, Vol. 22, No. 3, 317–322, 2016.

[38] Kipp, J., F. R. Lux, T. Pürling, A. Morrison, S. Blügel, D. Pinna, and Y. Mokrousov, "Machine learning inspired models for hall effects in non-collinear magnets," *Machine Learning: Science and Technology*, Vol. 5, No. 2, 025060, 2024.

[39] Schaal, C., S. Tai, and A. Mal, "On the assumption of transverse isotropy of a honeycomb sandwich panel for NDT applications," in *Health Monitoring of Structural and Biological Systems 2017*, Vol. 10170, 428–435, 2017.

[40] Yuan, X.-W., Z. Yang, M.-J. Gou, M.-L. Yang, and X.-Q. Sheng, "A flexible and efficient method for the analysis of electromagnetic scattering by inhomogeneous objects with honeycomb structures," *IEEE Antennas and Wireless Propagation Letters*, Vol. 21, No. 3, 541–545, 2022.

[41] Liu, T., Y. Pang, M. Zhu, and S. Kobayashi, "Microporous Co@CoO nanoparticles with superior microwave absorption properties," *Nanoscale*, Vol. 6, No. 4, 2447–2454, 2014.

[42] Ollendorff, F., "Magnetostatik der massekerne," *Archiv für Elektrotechnik*, Vol. 25, 436–447, 1931.